HHS Public Access

Author manuscript

Exp Eye Res. Author manuscript; available in PMC 2021 April 01.

Published in final edited form as:

Exp Eye Res. 2020 April ; 193: 107978. doi:10.1016/j.exer.2020.107978.

Neuroretinal rim response to transient changes in intraocular pressure in healthy non-human primate eyes

Laura P. Pardon[a], **Ronald S. Harwerth**[a], **Nimesh B. Patel**[a]

[a]University of Houston, College of Optometry 4901 Calhoun Road, Houston, TX 77204-2020

Abstract

Optic nerve head (ONH) neuroretinal rim thickness, quantified as minimum rim width (BMO-MRW), is a sensitive measure for assessing early glaucomatous disease. The BMO-MRW is sensitive to transient fluctuations in intraocular pressure (IOP), but the time course over which BMO-MRW decreases and recovers with changes in IOP remains unknown. The goal of this study was to investigate the dynamics of BMO-MRW changes over 2-hour periods of mild or moderate IOP elevation, and subsequent recovery, in healthy non-human primate eyes. Eight non-human primates were included in the study. For each animal, in two different sessions separated by at least 2 weeks, the anterior chamber IOP of one eye was maintained at either 25 mmHg or 40 mmHg for 2 hours and, subsequently, at 10 mmHg for 2 hours. For the duration of anterior chamber cannulation, optical coherence tomography (OCT) radial scans centered on the ONH were acquired every 5 min and used to quantify BMO-MRW. An exponential decay or rise to maximum function was used to determine the extent and rate of structural change. Additionally, Bruch's membrane opening (BMO) area, BMO height/displacement, and BMO-referenced anterior lamina cribrosa surface depth (BMO-ALCSD) were computed from radial scans. A circular scan was used to quantify retinal nerve fiber layer thickness (RNFLT) and circumpapillary choroid thickness. The primary results demonstrated that the BMO-MRW changed over an extended duration, while BMO displacement was rapid and remained stable with sustained IOP. The mean maximum predicted BMO-MRW thinning following 2 hours of IOP elevation was significantly related to pressure (34.2 ± 13.8 μm for an IOP of 25 mmHg vs 40.5 ± 12.6 μm for 40 mmHg, $p = 0.03$). The half-life for BMO-MRW thinning was 21.9 ± 9.2 min for 25 mmHg and 20.9 ± 4.2 min for 40 mmHg, not significantly different between IOP levels ($p = 0.76$). Subsequently, after 2 hours of IOP at 10 mmHg, all animals exhibited partial recovery of BMO-MRW with similar degrees of persistent residual thinning for the two IOP levels (21.5 ± 13.7 vs 21.0 ± 12.3 μm, $p = 0.88$). Similar to BMO-MRW, choroid thickness exhibited gradual thinning with IOP elevation and residual thinning following IOP reduction. However, there was no significant change in BMO area or BMO-ALCSD in either experimental session. The RNFLT gradually decreased over the duration of IOP elevation, with continued decreases following IOP

Correspondence: Laura Pardon, University of Houston, College of Optometry, 4901 Calhoun Road, Houston, TX 77204-2020, lppardon@central.uh.edu.

Declarations of interest (all authors): None

reduction for the 40 mmHg session, resulting in total changes from baseline of −2.24 ± 0.81 and −2.45 ± 1.21 μm for 25 and 40 mmHg, respectively ($p < 0.001$). The sum of the results demonstrate that the ONH neural tissue is sensitive to changes in IOP, the effects of which are gradual over an extended time course and different for increased vs. decreased pressure. Understanding the duration over which IOP influences BMO-MRW has important implications for studies investigating the effects of IOP on the ONH. Additionally, individual variability in ONH response to IOP may improve our understanding of the risk and progression of disease.

Keywords

intraocular pressure; optic nerve head; neuroretinal rim; minimum rim width; optical coherence tomography; non-human primate

1. Introduction

Glaucoma is a group of optic neuropathies characterized by progressive vision loss and structural changes to the optic nerve head (ONH) and retinal ganglion cell- (RGC-) containing layers of the retina. Though the mechanism underlying glaucoma remains elusive, intraocular pressure (IOP) is known to be a major risk factor for disease.

The ONH, a relative weak point in the posterior aspect of the globe, is susceptible to the influence of IOP and has been described as the initial site of damage in glaucoma (Downs, 2015; Howell et al., 2007; Quigley et al., 1983). ONH parameters, quantified using optical coherence tomography (OCT), have been shown to change early in disease. In fact, the ONH minimum rim width (BMO-MRW), a measure of the neuroretinal rim, thins prior to other RGC-containing layers such as the retinal nerve fiber layer (RNFL)(Chauhan et al., 2013; He et al., 2014; Ivers et al., 2015; Patel et al., 2014; Reis et al., 2012). These findings suggest that BMO-MRW may have utility in detecting early stages of disease. It has been proposed that early BMO-MRW changes occur as a result of compression and/or stretching of axon bundles within the ONH (Fortune et al., 2016b), but the temporal relationships between BMO-MRW and IOP have not been well-defined. These relationships are necessary to evaluate the general hypothesis that IOP-associated changes of the neuroretinal rim are related to the health of the eye and are a harbinger for IOP susceptibility in glaucoma.

Non-human primates (NHP) are an excellent model for studying ONH structural changes in response to IOP and experimental glaucoma because their ONH anatomy is very similar to that of humans. Studies in healthy NHP have demonstrated that exposure to short-duration changes in IOP result in substantial changes to the neuroretinal rim (Patel et al., 2018; Strouthidis et al., 2011). In our previous work, using 10 mmHg increments in IOP at 10 min intervals, significant changes in ONH BMO-MRW, Bruch's membrane opening (BMO) position, and choroid thickness were seen. While most of these structural measures returned to baseline when IOP was returned to 10 mmHg, there was significant residual thinning of BMO-MRW with IOP reduction (Patel et al., 2018). However, the short periods of IOP challenge did not allow an assessment of neuroretinal rim tissue dynamics with modulation of IOP. As a result, it is not known whether the full extent of neuroretinal rim thinning/recovery was achieved, or if the rim tissue would continue to thin/recover over a longer

period. Establishing the dynamics of neuroretinal rim change with short-term, sustained IOP modulation has important implications for both glaucoma pathophysiology and clinical practice. Therefore, the present investigations were undertaken to determine these effects over 2-hour periods of mild and moderate IOP elevation, and subsequent IOP reduction, in healthy NHP eyes.

2. Material and methods

2.1 Subjects

Eight healthy NHP (*Macaca mulatta*) were included in the study. The subjects included six males and two females, ranging in age from 4.8 to 5.8 years (mean age 5.6 years). For each subject, one eye was used in the study. Experimental procedures and animal care protocols were approved by the Institutional Animal Care and Use Committee at the University of Houston and adhered to the National Institutes of Health guidelines for the care and use of laboratory animals.

2.2 Animal Preparation

Prior to all experimental sessions, animals were anesthetized via intramuscular injections of ketamine (20–25 mg/kg) and xylazine (0.8–0.9 mg/kg), and were given a subcutaneous injection of atropine sulfate (0.04 mg/kg). Hourly doses of ketamine (20–25 mg/kg/hr) and xylazine (0.4–0.5 mg/kg/hr) were administered to maintain sedation. For the duration of anesthesia, heart rate, partial pressure of oxygen, blood pressure, and body temperature were continuously monitored as described previously (Patel et al., 2018).

Following administration of anesthesia, pupils were dilated with 1% tropicamide. The eyelids and ocular surface were cleaned with 5% ophthalmic betadine (Alcon Laboratories, Fort Worth, TX); following two minutes of betadine exposure, eyes were rinsed with sterile balanced salt solution (BSS, Alcon Laboratories, Fort Worth, TX). Mouth and occipital bars were used to stabilize the animal's head, and a sterile speculum was used to keep the experimental eye open. A plano gas-permeable contact lens was placed on the eye in order to prevent corneal dehydration and maintain optical clarity. At the end of the experiment, topical broad spectrum antibiotics (polymyxin B/trimethoprim and moxifloxacin) were instilled in the eye to prevent infection.

2.3 Anterior Chamber Cannulation and IOP Control

The anterior chamber was cannulated using a 27G butterfly needle, approximately 0.5 mm from the limbus. The needle was connected to a pressure control system, consisting of a capacitive pressure transducer (Keller PR-41X, Keller America, Newport News, VA) and syringe pump (Cole-Parmer, Vernon Hills, IL), via sterile microtubing filled with BSS. The pressure transducer and syringe pump were placed at the same height as the cannulated eye. The system was controlled through a MATLAB (The Mathworks, Natick, MA) program, which sampled pressure at 5 Hz and adaptively altered the rate of the syringe pump inflow/outflow to maintain IOP. This system was calibrated as described previously (McAllister et al., 2018).

Two cannulation experiments, separated by at least 2 weeks, were performed on each animal in order to assess ONH response to both mild (25 mmHg) and moderate (40 mmHg) IOP elevations. A mild pressure elevation of 25 mmHg corresponds with the median IOP elevation following induction of experimental glaucoma, and 40 mmHg was selected as a moderate elevation at which there is no reduction in superficial vessel density (Patel et al., 2018). For all experimental sessions, IOP was initially set to 10 mmHg and allowed to stabilize for at least 15 minutes prior to IOP elevation. IOP was then maintained at either 1) 25 mmHg or 2) 40 mmHg for 2 hours, then at 10 mmHg for an additional 2 hours to assess recovery of ONH structure. In order to assess possible effects of anesthesia on BMO-MRW over time, a control cannulation experiment was performed on the contralateral eye of one animal, with IOP maintained at 10 mmHg for approximately 2 hours.

2.4 Optical Coherence Tomography

At least 2 weeks prior to scheduling any cannulation experiment, each animal was sedated to obtain baseline optical biometry (Lenstar LS900, Haag-Streit, Koeniz, Switzerland) and OCT scans (Spectralis, Heidelberg Engineering, Heidelberg, Germany). In order to quantify ONH parameters, 12- or 24-line, 20-degree radial scans centered on the ONH (averaging of 20 frames; Fig. 1A) were acquired. Additionally, 12-degree circular scans centered on the ONH (averaging of 100 frames; Fig. 1B) were obtained to quantify circumpapillary RNFL and choroid thickness. Transverse retinal scaling for each subject was calculated using a three-surface schematic eye as described previously (Patel et al., 2011).

For each cannulation experiment, the AutoRescan feature was used to acquire all scans at 5 min intervals for the duration of pressure control. Based on our previous observations of structural change with IOP, BMO-MRW analysis was performed for all acquired scans (i.e., every 5 min), while all other OCT parameters were analyzed every 30 min. All OCT images were exported in their raw format (*.vol) and analyzed using programs written in MATLAB.

2.5 Optic Nerve Head Analysis

For each radial B-scan, the internal limiting membrane (ILM) and Bruch's membrane (BM) segmentations were manually corrected for any segmentation errors. Following image compensation, performed using the equation described by Girard et al. (Girard et al., 2011a), the two points corresponding with the BMO location were selected for each B-scan. In addition, the anterior lamina cribrosa surface (ALCS) was manually delineated on each B-scan only in regions where it was clearly visible. All selected BMO points were used to determine a best-fit ellipse, and BMO area was calculated as the area of this ellipse. The BMO-MRW was quantified as the minimum distance from the BMO to the ILM (Fig. 1C). BMO height/displacement was calculated as the minimum distance from a 12-degree BM reference plane centered on the ONH, a location corresponding to that of the circular scan path used for RNFL and choroid thickness, to the BMO (Fig. 1C). The ALCS depth (BMO-ALCSD) was quantified as the minimum distance from a reference plane connecting the BMO points to the selected ALCS points (Fig. 1C), only using the ALCS data within the middle 50% of the BMO distance. In this two-dimensional approach, all selected ALCS points (pixels) falling within the middle 50% of the BMO distance were weighted equally towards determining global BMO-ALCSD.

2.6 Circumpapillary RNFL and Choroid Analysis

For each circular scan, the boundaries of the ILM, BM, and RNFL were manually corrected for segmentation errors (major retinal vessels were included in the RNFL segmentation), and the choroid/sclera border was manually delineated on compensated B-scans (Girard et al., 2011a). The mean circumpapillary RNFL and choroid thicknesses were calculated as the average thickness between the ILM and RNFL, and BM and choroid/sclera borders, respectively (Fig. 1D).

2.7 Statistical Analysis

Global values for each parameter were used for the analysis and are expressed as mean ± standard deviation. Statistical analysis was performed with GraphPad Prism 7 (GraphPad Software, Inc., San Diego, CA). To assess the half-life and extent of neuroretinal rim change during IOP elevation and recovery, BMO-MRW (quantified every 5 min) as a function of time was fit with exponential one phase decay (Eqn. 1) or one phase association (i.e., rise to maximum, Eqn. 2) functions, respectively, where y_0 is the value of y when x (time) = 0, plateau is the value of y when x = infinity, and k is the rate constant. Maximum predicted BMO-MRW change was calculated as y_0 – plateau (Eqn. 1), half-life (decay) and half-time (rise) were calculated as ln(2)/k, and residual BMO-MRW thinning was calculated as [y_0 (Eqn. 1) – plateau (Eqn. 2)]. A paired t-test was used to determine differences in baseline parameters and differences in parameters between the 25 and 40 mmHg experiments.

(exponential decay): $$y = (y_0 - \text{plateau}) * e^{-kx} + \text{plateau}$$ Equation 1

(exponential rise): $$y = y_0 + (\text{plateau}_{max} - y_0) * (1 - e^{-kx})$$ Equation 2

One-way ANOVA with repeated measures was used to determine whether OCT parameters (quantified every 30 min) changed over time, comparing: 1) time points during IOP elevation to baseline, 2) time points during IOP reduction to the final time point of IOP elevation, and 3) endpoint to baseline; a Sidak multiple comparisons correction was applied. Linear regression analysis was performed to determine relationships between maximum predicted BMO-MRW change, baseline BMO-MRW, half-life, and other OCT parameters as described below. For all analyses, the significance level was 0.05.

3. Results

All animals maintained good systemic health during the experiments and throughout the duration of the study, and no adverse ocular events occurred as a result of cannulation. For each animal, experimental sessions were separated in time by at least 2 weeks. There was no significant difference in baseline BMO-MRW ($p = 0.22$) or baseline RNFL thickness ($p = 0.72$) between the first and second experimental sessions, suggesting that neither elevating IOP for 2 hours nor cannulation results in permanent ONH structural effects.

3.1 Optic Nerve Head Parameters

Global MRW was quantified every 5 min in order to determine dynamic changes in neuroretinal rim structure with 2-hour mild or moderate IOP elevation and subsequent reduction. All animals demonstrated a gradual thinning of the neuroretinal rim with IOP elevation that tended to approach an asymptote after 2 hours. The animals with the greatest and least changes in BMO-MRW with IOP elevation are shown in Figure 2. The control experiment, performed on the contralateral eye of the animal with the greatest BMO-MRW change, demonstrated comparatively minimal decrease in BMO-MRW when IOP was maintained at 10 mmHg (Fig. 3). For the entire group of animals, best-fit exponential decay functions demonstrated a maximum predicted BMO-MRW change of 34.2 ± 13.8 and 40.5 ± 12.6 μm for the 25 and 40 mmHg experiments, respectively. Though the degree of BMO-MRW thinning differed substantially between animals, it was significantly greater with the higher pressure setting ($p = 0.029$). Mean half-life was 21.9 ± 9.2 min for 25 mmHg and 20.9 ± 4.2 min for 40 mmHg and did not significantly differ between the two pressures ($p = 0.76$).

When IOP was changed to 10 mmHg for an additional 2 hours, all animals exhibited some recovery of neuroretinal rim thickness. Rather than reach baseline BMO-MRW values, the BMO-MRW initially increased rapidly then approached a plateau. Best-fit exponential rise to maximum functions revealed similar amounts of residual BMO-MRW thinning for the 25 and 40 mmHg experiments, with residual thinning of 21.5 ± 13.7 and 21.0 ± 12.3 μm, respectively ($p = 0.88$). Likewise, there was no significant difference in half-time between the two sets of experiments ($p = 0.40$). Individual parameters for exponential decay and rise to maximum functions are shown in Table 1. For both the 25 and 40 mmHg experiments, there was a strong relationship between maximum predicted BMO-MRW change and residual BMO-MRW thinning ($R^2 = 0.92$ and 0.79, $p = 0.0001$ and 0.003, respectively; Fig. 4A). Likewise, there was a relationship between maximum predicted BMO-MRW change and baseline BMO-MRW ($R^2 = 0.62$ and 0.55, $p = 0.020$ and 0.035; Fig. 4C). The relationship between maximum BMO-MRW change and half-life was not statistically significant ($p > 0.07$) (Fig. 4B).

All other ONH parameters were quantified every 30 min. Mean values for OCT parameters quantified every 30 min are shown in Table 2, and changes in these parameters from baseline are depicted in Figure 5. There was a trend for BMO area to increase over time for the 40 mmHg experiments, however, this increase from baseline was minimal (0.018 ± 0.021 mm^2) and there was no significant change in BMO area over the 4-hour period for either set of experiments ($p > 0.07$; Fig. 5C). Similarly, BMO-ALCSD did not significantly change during either experiment ($p > 0.05$; Fig. 5E). As in previous studies, some subjects demonstrated an increase in BMO-ALCSD with elevated IOP whereas other subjects exhibited a decrease in BMO-ALCSD (Agoumi et al., 2011; Fazio et al., 2016; Ivers et al., 2016; Strouthidis et al., 2011; Yang et al., 2009)(Fig. 6). While the lamina cribrosa can be displaced posteriorly in response to elevated IOP exerting an outward force on the globe, anterior displacement can occur if the elevated IOP results in sufficient scleral expansion due to hoop stress, essentially pulling the lamina taught and inward (Sigal et al., 2011a; Sigal et al., 2011b). Though there was no significant change in BMO area or BMO-ALCSD when

considering the mean data, it is possible that individual animals demonstrate changes in these parameters that are associated with structural changes in the neural rim tissue. For example, an animal with an increase in BMO area may exhibit a greater extent of BMO-MRW thinning as a result of the same number of axons being spread over an increased area compared with an animal in which BMO area did not change. Likewise, greater posterior movement of the BMO-ALCSD could result in greater strain and stretching of RGC axons, manifesting as greater BMO-MRW thinning. To better understand whether these mechanisms may contribute to the observed neuroretinal rim thinning, we investigated relationships between maximum change in BMO-MRW and maximum change in BMO area and BMO-ALCSD. Additionally, since it is possible that a greater change in BMO area or BMO-ALCSD may be associated with a shorter half-life for BMO-MRW change, relationships between half-life and maximum change in BMO area and BMO-ALCSD were assessed. There was no significant relationship between maximum change in BMO-MRW or half-life and either of these parameters ($p > 0.38$). Although BMO area did not significantly change, it is possible that the scleral canal expands posterior to the BMO in response to elevated IOP. Though such changes are not currently quantifiable using OCT, they would likely impact axon configuration at the neuroretinal rim and, therefore, BMO-MRW measures.

Contrary to BMO-MRW, BMO height changed rapidly with IOP modulation and remained stable when IOP was held constant (Fig. 5D). During IOP elevation, all time points demonstrated a significant increase in BMO height magnitude (i.e., posterior BMO deflection) compared to baseline for both sets of experiments ($p < 0.01$); this change was approximately 22.0 ± 10.4 μm for 25 mmHg and 27.2 ± 16.3 μm for 40 mmHg. When IOP was reduced to 10 mmHg, BMO height rapidly changed to approximately baseline values. All time points at 10 mmHg demonstrated a smaller magnitude (i.e., more anterior) BMO height compared with the final time point of IOP elevation for both sets of experiments ($p < 0.005$). There was no significant difference between baseline and endpoint BMO height with either mild or moderate IOP elevation ($p > 0.15$). A greater posterior displacement of the BMO with IOP elevation could signify a peripapillary sclera that is more compliant and therefore an ONH that is more susceptible to structural change with IOP. Since change in BMO height was found to occur rapidly, it is possible that animals with a larger change in BMO height may exhibit more rapid thinning of the neuroretinal rim (i.e., a shorter half-life). The relationship between maximum change in BMO-MRW and maximum change in BMO height was not statistically significant ($p > 0.17$). Though there was a significant relationship between half-life and BMO height for the 25 mmHg experiment ($R^2 = 0.53$, $p = 0.04$; Fig. 4D), this relationship was not significant for the 40 mmHg experiment ($p = 0.44$).

3.2 Circumpapillary Retinal Nerve Fiber Layer Thickness

Retinal nerve fiber layer thickness demonstrated a gradual reduction from baseline over the 4-hour period (Fig. 5B). For both the 25 and 40 mmHg experiments, RNFL thickness was significantly reduced from baseline at both 1.5 and 2 hours of IOP elevation ($p < 0.05$). Following pressure reduction to 10 mmHg, there was no further change in RNFL thickness for the 25 mmHg experiments ($p = 0.30$). However, there was continued thinning of the RNFL for the 40 mmHg experiments at all four time points of IOP reduction ($p < 0.05$). At

endpoint, RNFL thickness was significantly reduced from baseline ($p < 0.001$), with mean reductions of 2.24 ± 0.81 and 2.45 ± 1.21 μm for the 25 and 40 mmHg experiments, respectively. Since BMO-MRW and RNFL consist of the same population of RGC axons, we investigated the relationship between maximum change in BMO-MRW and maximum change in RNFL thickness and determined that there was no significant relationship ($p > 0.50$).

3.3 Circumpapillary Choroid Thickness

Changes in circumpapillary choroid thickness with IOP modulation followed a similar pattern to changes in BMO-MRW, with a gradual decrease in choroid thickness during IOP elevation and residual choroidal thinning following IOP reduction (Fig. 5F). During IOP elevation, choroid thickness was significantly reduced from baseline at all time points ($p < 0.05$); at 2 hours of IOP elevation, a greater degree of thinning occurred with moderate IOP elevation (20.4 ± 7.2 μm) than with mild IOP elevation (13.4 ± 4.9 μm, $p = 0.02$). Following IOP reduction to 10 mmHg, there was no further change in choroid thickness for the 25 mmHg experiments ($p = 0.26$). There was, however, a significant recovery of choroid thickness for the 40 mmHg experiments at all subsequent time points ($p < 0.05$). For both sets of experiments, there was a significant reduction in choroid thickness at endpoint relative to baseline ($p < 0.002$); this difference was similar for the 25 and 40 mmHg experiments, with residual thinning of 12.1 ± 4.4 and 10.7 ± 5.8 μm, respectively. Our finding that changes in circumpapillary choroid thickness mirror changes in the BMO-MRW lead to the question of whether the observed BMO-MRW thinning is related to changes in choroid thickness. The relationship between maximum change in BMO-MRW and maximum change in circumpapillary choroid thickness, however, was not statistically significant ($p > 0.80$).

4. Discussion

The present study demonstrated that the neuroretinal rim, quantified as minimum rim width (BMO-MRW), thins gradually over a prolonged time course when IOP is elevated and held at a mild-to-moderate level and approaches an asymptote with approximately two hours of IOP elevation. In addition, the neuroretinal rim does not return to baseline, but rather approaches an asymptote, with two hours of relatively low IOP. Our results also show that the pressure-induced neuroretinal rim changes are not related to deflection of the lamina or BMO size/position, nor are they mirrored by RNFL thickness.

Rather than symmetrically returning to baseline within the two hours following lowering of IOP, the neuroretinal rim exhibited residual thinning in all animals. The BMO-MRW did, however, recover to baseline values at later follow-up scan sessions, suggesting that the thinning cannot be attributed to axonal loss. It is possible that RGC axons are stretched and/or compressed in the presence of elevated IOP; in fact, this has been hypothesized to play a key role in the pathophysiology of glaucoma (Fortune et al., 2016b). All RGC axons pass through the lamina cribrosa, and displacement of the lamina would presumably result in stress to and/or stretching of RGC axons. Posterior displacement of the ALCS is one of the earliest signs of glaucomatous damage, occurring prior to RNFL thinning and concurrently

with a decrease in BMO-MRW (He et al., 2014; Ivers et al., 2015; Strouthidis et al., 2011). While this supports the notion that axonal stretching may occur early in disease, a significant change was not found for BMO-ALCSD with short-term IOP modulation in healthy eyes, nor was a relationship observed between maximum change in BMO-ALCSD and either maximum change in BMO-MRW or half-life. Therefore, while axonal compression cannot be ruled out, it seems unlikely that the observed decrease in BMO-MRW in the present study was a result of axonal stretching from displacement of the lamina. Our finding that some subjects exhibit posterior ALCS displacement in response to IOP elevation whereas others show anterior displacement is consistent with previous studies (Agoumi et al., 2011; Fazio et al., 2016; Ivers et al., 2016; Strouthidis et al., 2011; Yang et al., 2009) and can be explained by individual differences in ocular biomechanical responses to competing translaminar pressure difference and hoop strain forces. The parameter BMO-MRW is an anatomical measure of neuroretinal rim thickness and does not estimate stresses or strains to ONH tissue. Though our findings suggest that neuroretinal rim tissue exhibits viscoelastic properties in response to IOP, this was not assessed in the present study. However, there is active research measuring stress/strain responses of the ONH, lamina, and peripapillary sclera in post-mortem eyes and *in vivo*, which will further enhance our understanding of tissue responses to IOP (Beotra et al., 2018; Boote et al., 2019; Downs, 2015; Fazio et al., 2019; Girard et al., 2016; Tran et al., 2017).

The BMO exhibited posterior deflection with elevated IOP that returned to baseline following IOP reduction, as has been described previously (Patel et al., 2018; Strouthidis et al., 2011). This change in BMO location occurred rapidly with change in IOP and remained stable while pressure was held constant, in contrast to BMO-MRW which changed gradually over a prolonged period of time. It is possible that posterior deflection of the BMO is the result of an increase in axial length with IOP elevation. Though axial length was not measured in the present study due to time constraints, data from 7 healthy animals in our lab suggests that axial length increases approximately 60 μm when IOP is elevated in graded steps from 10 to 40 mmHg over a period of 10 min and decreases when IOP is then returned to 10 mmHg (data not shown). It is therefore likely that there was some degree of axial globe elongation and subsequent shortening in our longer-duration experiments. While the axial position of the BMO changed rapidly with IOP, there was no observed lateral expansion of the BMO with elevated IOP. The finding that there is no significant change in BMO area with transient IOP elevation is in accordance with other studies (Burgoyne et al., 1995; Patel et al., 2018; Sharma et al., 2017; Strouthidis et al., 2011). We hypothesized that individual changes in BMO size and/or anterior-posterior position may be associated with the extent/rate of BMO-MRW change (due to redistribution of axons over a larger area or a more compliant sclera, respectively), however, these relationships were not statistically significant. Though the BMO area did not change, it is possible that the scleral canal expands posterior to the BMO in response to IOP-induced hoop stress. Expansion of the scleral canal would presumably cause axons to be displaced posteriorly and laterally, thereby resulting in thinning of the BMO-MRW. Though scleral expansion posterior to the BMO could not be quantified using OCT, previous studies in post-mortem human and monkey eyes describe scleral expansion at increased levels of IOP (Bellezza et al., 2003; Ma et al., 2019).

In addition to RGC axons, the ONH is composed of vasculature, glial tissue, and extracellular matrix. It has previously been shown that peripapillary superficial vessel density, derived from OCT angiography, remains unchanged in healthy eyes up to 40 mmHg, the highest IOP setting in the present study (Fortune et al., 2019; Patel et al., 2018). Additionally, it was determined to be improbable that the degree of BMO-MRW thinning observed with graded increases in IOP was a result of changes in blood vessel caliber (Patel et al., 2018). The finding that there was a similar degree of residual thinning for both the 25 and 40 mmHg experiments suggests that a common component of the neuroretinal rim is temporarily altered/depleted for both mild and moderate IOP elevations. One possibility is that extracellular fluid is reduced following sustained short-term IOP elevation. However, previous calculations by Burgoyne et al. have estimated that loss of extracellular fluid would only result in a 5 μm change to the surface of the optic disc, substantially less than the approximately 20 μm of residual thinning exhibited (Burgoyne et al., 1995). Though the exact cause of neuroretinal rim thinning with IOP elevation is unknown, we hypothesize that the thinning reflects changes to the extracellular environment. Astrocytes are the primary glial cell type in the ONH and provide structural and physiological support to RGC axons. Previous studies have demonstrated that astrocytes have mechanosensitive properties that allow them to respond to changes in IOP (Beckel et al., 2014; Choi et al., 2015), as well as aquaporin channels that are involved in fluid exchange with the extracellular space (Goodyear et al., 2009; Nagelhus et al., 1998). It is possible that the observed neuroretinal rim thinning with elevated IOP is multifactorial and may reflect a combination of astrocyte remodeling, redistribution of extracellular fluid, and changes in axon distribution resulting from posterior scleral expansion, though this remains to be investigated.

The anatomy of the peripapillary choroid is thought to influence biomechanics of the ONH (Feola et al., 2018). In the present study, we determined that circumpapillary choroid thickness followed a similar pattern as BMO-MRW with IOP elevation and subsequent reduction; this result is in agreement with previous studies that have demonstrated thinning of the choroid with acute IOP elevation and thickening of the choroid following IOP reduction (Akahori et al., 2017; Hata et al., 2012; Kara et al., 2013; Usui et al., 2013; Wang et al., 2016). Though it is not clear why there was a significant recovery of choroid thickness for the 40 mmHg experiments but not for the 25 mmHg experiments, a greater rebound for the higher pressure elevation was also observed for neuroretinal rim recovery. However, there was no significant relationship between maximum change in circumpapillary choroid thickness and maximum change in BMO-MRW.

Previous studies have reported a small, but significant, reduction in RNFL thickness with acute elevations in IOP (Fortune et al., 2009). The current study also observed a significant decrease in RNFL thickness with elevated IOP, however, the continued RNFL thinning during a period of reduced IOP was unexpected. It is possible that the small degree RNFL thinning may reflect diurnal variations rather than an effect related to IOP. Though not statistically significant for global measures, decreases in RNFL thickness from morning to evening have previously been reported in healthy humans (Ashraf and Nowroozzadeh, 2014; Sharifipour et al., 2016). It is also possible that the thinning of the RNFL could be a secondary effect of anesthesia, which cannot be accounted for. There was no relationship between RNFL and BMO-MRW change, supporting previous findings that thinning of these

two structures occurs independently (Fortune et al., 2016a; Fortune et al., 2016b; He et al., 2014; Patel et al., 2018; Patel et al., 2014).

The finding that the extent/rate of BMO-MRW thinning with IOP elevation is not related to deflection of the lamina, BMO size or position, or RNFL thickness suggests that neuroretinal rim response to IOP is an independent parameter that can provide additional information regarding ONH susceptibility to IOP. There was a considerable degree of inter-individual variability in the extent of BMO-MRW thinning with IOP elevation and rebound of structure following IOP reduction. Individual differences in ONH response to IOP have been described previously and may reflect differences in the biomechanical properties of ONH and peripapillary structures, such as the lamina cribrosa and sclera (Burgoyne et al., 1995; Strouthidis et al., 2011). Previous models have suggested that material properties of these structures, particularly the peripapillary sclera, play an important role in determining ONH response to acute changes in IOP (Sigal et al., 2009). Scleral stiffness has been shown to increase with age and disease process (Coudrillier et al., 2015a; Coudrillier et al., 2015b; Coudrillier et al., 2012; Downs et al., 2005; Fazio et al., 2014; Girard et al., 2009, 2011b). While biomechanical properties were not assessed in the present study, it stands to reason that in the presence of elevated IOP, compression of neuroretinal rim tissue against a stiffer sclera would result in a greater magnitude of neuroretinal rim thinning (and less neuroretinal rim recovery) compared with a more compliant sclera. We found that animals with a greater maximum change in BMO-MRW also tended to exhibit greater residual thinning, whereas animals with lesser degrees of BMO-MRW thinning tended to demonstrate a more robust rebound. Whether the former is related to increased scleral stiffness, and potentially increased risk of glaucomatous damage with elevated IOP, remains to be investigated.

Several human studies have investigated changes in ONH structure with acute IOP elevations using ophthalmodynamometry in healthy and glaucomatous eyes, though longer duration studies are needed to fully investigate neuroretinal rim properties. In one study, BMO-MRW was found to decrease in glaucomatous but not healthy eyes following IOP elevation (Sharma et al., 2017). Another study demonstrated a greater degree of prelaminar tissue thinning in healthy eyes compared with glaucomatous eyes (Agoumi et al., 2011). Both studies involved very brief elevations of IOP of approximately 2–3 minutes, which may explain their conflicting results. This duration may be too short to be meaningful, as the half-life for BMO-MRW thinning in NHP is approximately 20 minutes. Therefore, it is anticipated that longer durations of IOP elevation will reveal significant reductions in neuroretinal rim thickness in both healthy and glaucomatous eyes, and that the dynamics of thinning will differ based on disease status and/or risk of disease. If such differences in neuroretinal rim behavior are observed, assessment of neuroretinal rim response to sustained IOP elevation and/or reduction with IOP-lowering medications could potentially be used clinically to identify individuals at a high risk of developing glaucoma and/or glaucoma patients with a higher risk of progression for whom more aggressive treatment (i.e., a lower target IOP) may be indicated. According to the results of the current study, exposure to longer durations of mild-to-moderate IOP elevation should be safe, as there was no significant difference in BMO-MRW or RNFL thickness between the first and second experimental sessions.

There are several limitations to the present study. The use of anesthesia was required to perform cannulation experiments, and it is possible that this influenced ocular physiology; however, a control experiment in one animal agrees with previous shorter-duration findings that there is minimal change in neuroretinal rim structure over time when animals are anesthetized and IOP maintained at 10 mmHg (Strouthidis et al., 2011). Though at least 15 min were allowed for the eye to equilibrate at 10 mmHg prior to increasing IOP, it is possible that a longer duration would have led to more stable baseline measures, particularly if a given animal had a higher pre-cannulation IOP. Since each eye was only tested once, the repeatability of BMO-MRW thinning and recovery with IOP modulation remains unknown; this will be important to establish if neuroretinal rim dynamics have potential applications for glaucoma risk assessment. However, based on a previous study in which change in mean position of the disc with IOP modulation was investigated and repeated (Burgoyne et al., 1995), the findings are expected to be repeatable on subsequent cannulations. Additionally, we were not able to assess the width of the scleral canal using our methods and were therefore unable to determine whether neuroretinal rim thinning is associated with scleral canal expansion. While there are many anatomical similarities between NHP and human eyes, the NHP eye exhibits a shorter axial length and thinner peripapillary scleral thickness (Downs et al., 2002; Girkin et al., 2017; Jonas et al., 2011); as a result of these differences, the NHP eye likely exhibits more compliant behavior than the human eye. This study included only young and healthy animals, and determining how neuroretinal rim dynamics are altered with age and disease will be the focus of future investigations.

5. Conclusions

In conclusion, this study confirms that the neuroretinal rim is sensitive to mild and moderate elevations in IOP and demonstrates that the neuroretinal rim changes over a prolonged time course with substantial residual thinning following IOP reduction and that there is considerable variability among individuals with regards to the extent of thinning and recovery. Characteristics of BMO-MRW dynamics with IOP modulation may provide important information regarding ONH compliance and risk of structural damage with prolonged IOP elevation.

Acknowledgements

The authors thank Dr. Faith McAllister for her assistance with optical coherence tomography segmentations.

Funding: This work was supported by the National Institutes of Health [R01 EY029229, P30 EY007551] and the University of Houston Mary Murphy Research Endowment.

References

Agoumi Y, Sharpe GP, Hutchison DM, Nicolela MT, Artes PH, Chauhan BC, 2011 Laminar and prelaminar tissue displacement during intraocular pressure elevation in glaucoma patients and healthy controls. Ophthalmology 118, 52–59. [PubMed: 20656352]

Akahori T, Iwase T, Yamamoto K, Ra E, Terasaki H, 2017 Changes in Choroidal Blood Flow and Morphology in Response to Increase in Intraocular Pressure. Invest Ophthalmol Vis Sci 58, 5076–5085. [PubMed: 28980002]

Ashraf H, Nowroozzadeh MH, 2014 Diurnal variation of retinal thickness in healthy subjects. Optom Vis Sci 91, 615–623. [PubMed: 24811843]

Beckel JM, Argall AJ, Lim JC, Xia J, Lu W, Coffey EE, Macarak EJ, Shahidullah M, Delamere NA, Zode GS, Sheffield VC, Shestopalov VI, Laties AM, Mitchell CH, 2014 Mechanosensitive release of adenosine 5'-triphosphate through pannexin channels and mechanosensitive upregulation of pannexin channels in optic nerve head astrocytes: a mechanism for purinergic involvement in chronic strain. Glia 62, 1486–1501. [PubMed: 24839011]

Bellezza AJ, Rintalan CJ, Thompson HW, Downs JC, Hart RT, Burgoyne CF, 2003 Anterior scleral canal geometry in pressurised (IOP 10) and non-pressurised (IOP 0) normal monkey eyes. Br J Ophthalmol 87, 1284–1290. [PubMed: 14507767]

Beotra MR, Wang X, Tun TA, Zhang L, Baskaran M, Aung T, Strouthidis NG, Girard MJA, 2018 In Vivo Three-Dimensional Lamina Cribrosa Strains in Healthy, Ocular Hypertensive, and Glaucoma Eyes Following Acute Intraocular Pressure Elevation. Invest Ophthalmol Vis Sci 59, 260–272. [PubMed: 29340640]

Boote C, Sigal IA, Grytz R, Hua Y, Nguyen TD, Girard MJA, 2019 Scleral structure and biomechanics. Prog Retin Eye Res, 100773.

Burgoyne CF, Quigley HA, Thompson HW, Vitale S, Varma R, 1995 Measurement of optic disc compliance by digitized image analysis in the normal monkey eye. Ophthalmology 102, 1790–1799. [PubMed: 9098279]

Chauhan BC, O'Leary N, Almobarak FA, Reis AS, Yang H, Sharpe GP, Hutchison DM, Nicolela MT, Burgoyne CF, 2013 Enhanced detection of open-angle glaucoma with an anatomically accurate optical coherence tomography-derived neuroretinal rim parameter. Ophthalmology 120, 535–543. [PubMed: 23265804]

Choi HJ, Sun D, Jakobs TC, 2015 Astrocytes in the optic nerve head express putative mechanosensitive channels. Mol Vis 21, 749–766. [PubMed: 26236150]

Coudrillier B, Pijanka J, Jefferys J, Sorensen T, Quigley HA, Boote C, Nguyen TD, 2015a Collagen structure and mechanical properties of the human sclera: analysis for the effects of age. Journal of Biomechanical Engineering 137, 041006. [PubMed: 25531905]

Coudrillier B, Pijanka JK, Jefferys JL, Goel A, Quigley HA, Boote C, Nguyen TD, 2015b Glaucoma-related Changes in the Mechanical Properties and Collagen Micro-architecture of the Human Sclera. PLoS One 10, e0131396. [PubMed: 26161963]

Coudrillier B, Tian J, Alexander S, Myers KM, Quigley HA, Nguyen TD, 2012 Biomechanics of the human posterior sclera: age- and glaucoma-related changes measured using inflation testing. Invest Ophthalmol Vis Sci 53, 1714–1728. [PubMed: 22395883]

Downs JC, 2015 Optic nerve head biomechanics in aging and disease. Exp Eye Res 133, 19–29. [PubMed: 25819451]

Downs JC, Blidner RA, Bellezza AJ, Thompson HW, Hart RT, Burgoyne CF, 2002 Peripapillary scleral thickness in perfusion-fixed normal monkey eyes. Invest Ophthalmol Vis Sci 43, 2229–2235. [PubMed: 12091421]

Downs JC, Suh JK, Thomas KA, Bellezza AJ, Hart RT, Burgoyne CF, 2005 Viscoelastic material properties of the peripapillary sclera in normal and early-glaucoma monkey eyes. Invest Ophthalmol Vis Sci 46, 540–546. [PubMed: 15671280]

Fazio MA, Girard MJA, Lee W, Morris JS, Burgoyne CF, Downs JC, 2019 The Relationship Between Scleral Strain Change and Differential Cumulative Intraocular Pressure Exposure in the Nonhuman Primate Chronic Ocular Hypertension Model. Invest Ophthalmol Vis Sci 60, 4141–4150. [PubMed: 31598625]

Fazio MA, Grytz R, Morris JS, Bruno L, Gardiner SK, Girkin CA, Downs JC, 2014 Age-related changes in human peripapillary scleral strain. Biomech Model Mechanobiol 13, 551–563. [PubMed: 23896936]

Fazio MA, Johnstone JK, Smith B, Wang L, Girkin CA, 2016 Displacement of the Lamina Cribrosa in Response to Acute Intraocular Pressure Elevation in Normal Individuals of African and European Descent. Invest Ophthalmol Vis Sci 57, 3331–3339. [PubMed: 27367500]

Feola AJ, Nelson ES, Myers J, Ethier CR, Samuels BC, 2018 The Impact of Choroidal Swelling on Optic Nerve Head Deformation. Invest Ophthalmol Vis Sci 59, 4172–4181. [PubMed: 30120486]

Fortune B, Hardin C, Reynaud J, Cull G, Yang H, Wang L, Burgoyne CF, 2016a Comparing Optic Nerve Head Rim Width, Rim Area, and Peripapillary Retinal Nerve Fiber Layer Thickness to

Axon Count in Experimental Glaucoma. Invest Ophthalmol Vis Sci 57, OCT404–412. [PubMed: 27409499]

Fortune B, Reynaud J, Hardin C, Cull G, Wang L, Burgoyne C, 2019 Optic nerve head (ONH) hypercompliance and blood flow autoregulation dysfunction detected by OCT-angiography (OCTA) in early-stage experimental glaucoma. Invest Ophthalmol Vis Sci ARVO E-Abstract.

Fortune B, Reynaud J, Hardin C, Wang L, Sigal IA, Burgoyne CF, 2016b Experimental Glaucoma Causes Optic Nerve Head Neural Rim Tissue Compression: A Potentially Important Mechanism of Axon Injury. Invest Ophthalmol Vis Sci 57, 4403–4411. [PubMed: 27564522]

Fortune B, Yang H, Strouthidis NG, Cull GA, Grimm JL, Downs JC, Burgoyne CF, 2009 The effect of acute intraocular pressure elevation on peripapillary retinal thickness, retinal nerve fiber layer thickness, and retardance. Invest Ophthalmol Vis Sci 50, 4719–4726. [PubMed: 19420342]

Girard MJ, Beotra MR, Chin KS, Sandhu A, Clemo M, Nikita E, Kamal DS, Papadopoulos M, Mari JM, Aung T, Strouthidis NG, 2016 In Vivo 3-Dimensional Strain Mapping of the Optic Nerve Head Following Intraocular Pressure Lowering by Trabeculectomy. Ophthalmology 123, 1190–1200. [PubMed: 26992836]

Girard MJ, Strouthidis NG, Ethier CR, Mari JM, 2011a Shadow removal and contrast enhancement in optical coherence tomography images of the human optic nerve head. Invest Ophthalmol Vis Sci 52, 7738–7748. [PubMed: 21551412]

Girard MJ, Suh JK, Bottlang M, Burgoyne CF, Downs JC, 2009 Scleral biomechanics in the aging monkey eye. Invest Ophthalmol Vis Sci 50, 5226–5237. [PubMed: 19494203]

Girard MJ, Suh JK, Bottlang M, Burgoyne CF, Downs JC, 2011b Biomechanical changes in the sclera of monkey eyes exposed to chronic IOP elevations. Invest Ophthalmol Vis Sci 52, 5656–5669. [PubMed: 21519033]

Girkin CA, Fazio MA, Yang H, Reynaud J, Burgoyne CF, Smith B, Wang L, Downs JC, 2017 Variation in the Three-Dimensional Histomorphometry of the Normal Human Optic Nerve Head With Age and Race: Lamina Cribrosa and Peripapillary Scleral Thickness and Position. Invest Ophthalmol Vis Sci 58, 3759–3769. [PubMed: 28738420]

Goodyear MJ, Crewther SG, Junghans BM, 2009 A role for aquaporin-4 in fluid regulation in the inner retina. Visual neuroscience 26, 159–165. [PubMed: 19366470]

Hata M, Hirose F, Oishi A, Hirami Y, Kurimoto Y, 2012 Changes in choroidal thickness and optical axial length accompanying intraocular pressure increase. Jpn J Ophthalmol 56, 564–568. [PubMed: 22886000]

He L, Yang H, Gardiner SK, Williams G, Hardin C, Strouthidis NG, Fortune B, Burgoyne CF, 2014 Longitudinal detection of optic nerve head changes by spectral domain optical coherence tomography in early experimental glaucoma. Invest Ophthalmol Vis Sci 55, 574–586. [PubMed: 24255047]

Howell GR, Libby RT, Jakobs TC, Smith RS, Phalan FC, Barter JW, Barbay JM, Marchant JK, Mahesh N, Porciatti V, Whitmore AV, Masland RH, John SW, 2007 Axons of retinal ganglion cells are insulted in the optic nerve early in DBA/2J glaucoma. The Journal of Cell Biology 179, 1523–1537. [PubMed: 18158332]

Ivers KM, Sredar N, Patel NB, Rajagopalan L, Queener HM, Twa MD, Harwerth RS, Porter J, 2015 In Vivo Changes in Lamina Cribrosa Microarchitecture and Optic Nerve Head Structure in Early Experimental Glaucoma. PLoS One 10, e0134223. [PubMed: 26230993]

Ivers KM, Yang H, Gardiner SK, Qin L, Reyes L, Fortune B, Burgoyne CF, 2016 In Vivo Detection of Laminar and Peripapillary Scleral Hypercompliance in Early Monkey Experimental Glaucoma. Invest Ophthalmol Vis Sci 57, Oct388–403. [PubMed: 27409498]

Jonas JB, Hayreh SS, Yong T, 2011 Thickness of the lamina cribrosa and peripapillary sclera in Rhesus monkeys with nonglaucomatous or glaucomatous optic neuropathy. Acta Ophthalmol 89, e423–427. [PubMed: 21332675]

Kara N, Baz O, Altan C, Satana B, Kurt T, Demirok A, 2013 Changes in choroidal thickness, axial length, and ocular perfusion pressure accompanying successful glaucoma filtration surgery. Eye (Lond) 27, 940–945. [PubMed: 23743533]

Ma Y, Pavlatos E, Clayson K, Pan X, Kwok S, Sandwisch T, Liu J, 2019 Mechanical Deformation of Human Optic Nerve Head and Peripapillary Tissue in Response to Acute IOP Elevation. Invest Ophthalmol Vis Sci 60, 913–920. [PubMed: 30835783]

McAllister F, Harwerth R, Patel N, 2018 Assessing the True Intraocular Pressure in the Non-human Primate. Optom Vis Sci 95, 113–119. [PubMed: 29370024]

Nagelhus EA, Veruki ML, Torp R, Haug FM, Laake JH, Nielsen S, Agre P, Ottersen OP, 1998 Aquaporin-4 water channel protein in the rat retina and optic nerve: polarized expression in Muller cells and fibrous astrocytes. J Neurosci 18, 2506–2519. [PubMed: 9502811]

Patel N, McAllister F, Pardon L, Harwerth R, 2018 The effects of graded intraocular pressure challenge on the optic nerve head. Exp Eye Res 169, 79–90. [PubMed: 29409880]

Patel NB, Luo X, Wheat JL, Harwerth RS, 2011 Retinal nerve fiber layer assessment: area versus thickness measurements from elliptical scans centered on the optic nerve. Invest Ophthalmol Vis Sci 52, 2477–2489. [PubMed: 21220552]

Patel NB, Sullivan-Mee M, Harwerth RS, 2014 The relationship between retinal nerve fiber layer thickness and optic nerve head neuroretinal rim tissue in glaucoma. Invest Ophthalmol Vis Sci 55, 6802–6816. [PubMed: 25249610]

Quigley HA, Hohman RM, Addicks EM, Massof RW, Green WR, 1983 Morphologic changes in the lamina cribrosa correlated with neural loss in open-angle glaucoma. Am J Ophthalmol 95, 673–691. [PubMed: 6846459]

Reis AS, O'Leary N, Yang H, Sharpe GP, Nicolela MT, Burgoyne CF, Chauhan BC, 2012 Influence of clinically invisible, but optical coherence tomography detected, optic disc margin anatomy on neuroretinal rim evaluation. Invest Ophthalmol Vis Sci 53, 1852–1860. [PubMed: 22410561]

Sharifipour F, Farrahi F, Moghaddasi A, Idani A, Yaseri M, 2016 Diurnal Variations in Intraocular Pressure, Central Corneal Thickness, and Macular and Retinal Nerve Fiber Layer Thickness in Diabetics and Normal Individuals. J Ophthalmic Vis Res 11, 42–47. [PubMed: 27195084]

Sharma S, Tun TA, Baskaran M, Atalay E, Thakku SG, Liang Z, Milea D, Strouthidis NG, Aung T, Girard MJ, 2017 Effect of acute intraocular pressure elevation on the minimum rim width in normal, ocular hypertensive and glaucoma eyes. Br J Ophthalmol.

Sigal IA, Flanagan JG, Tertinegg I, Ethier CR, 2009 Modeling individual-specific human optic nerve head biomechanics. Part II: influence of material properties. Biomech Model Mechanobiol 8, 99–109. [PubMed: 18301933]

Sigal IA, Yang H, Roberts MD, Burgoyne CF, Downs JC, 2011a IOP-induced lamina cribrosa displacement and scleral canal expansion: an analysis of factor interactions using parameterized eye-specific models. Invest Ophthalmol Vis Sci 52, 1896–1907. [PubMed: 20881292]

Sigal IA, Yang H, Roberts MD, Grimm JL, Burgoyne CF, Demirel S, Downs JC, 2011b IOP-induced lamina cribrosa deformation and scleral canal expansion: independent or related? Invest Ophthalmol Vis Sci 52, 9023–9032. [PubMed: 21989723]

Strouthidis NG, Fortune B, Yang H, Sigal IA, Burgoyne CF, 2011 Effect of acute intraocular pressure elevation on the monkey optic nerve head as detected by spectral domain optical coherence tomography. Invest Ophthalmol Vis Sci 52, 9431–9437. [PubMed: 22058335]

Tran H, Grimm J, Wang B, Smith MA, Gogola A, Nelson S, Tyler-Kabara E, Schuman J, Wollstein G, Sigal IA, 2017 Mapping in-vivo optic nerve head strains caused by intraocular and intracranial pressures. Proc SPIE Int Soc Opt Eng 10067.

Usui S, Ikuno Y, Uematsu S, Morimoto Y, Yasuno Y, Otori Y, 2013 Changes in axial length and choroidal thickness after intraocular pressure reduction resulting from trabeculectomy. Clin Ophthalmol 7, 1155–1161. [PubMed: 23807833]

Wang YX, Jiang R, Ren XL, Chen JD, Shi HL, Xu L, Wei WB, Jonas JB, 2016 Intraocular pressure elevation and choroidal thinning. Br J Ophthalmol 100, 1676–1681. [PubMed: 27016503]

Yang H, Downs JC, Sigal IA, Roberts MD, Thompson H, Burgoyne CF, 2009 Deformation of the normal monkey optic nerve head connective tissue after acute IOP elevation within 3-D histomorphometric reconstructions. Invest Ophthalmol Vis Sci 50, 5785–5799. [PubMed: 19628739]

HIGHLIGHTS

- Changes in intraocular pressure result in rapid changes in the neuroretinal rim
- The neuroretinal rim continues to change over a period of 2 hrs with sustained IOP
- Residual thinning of the neuroretinal rim persists after 2 hrs of IOP reduction
- There is individual variability in the rate and extent of rim tissue thinning

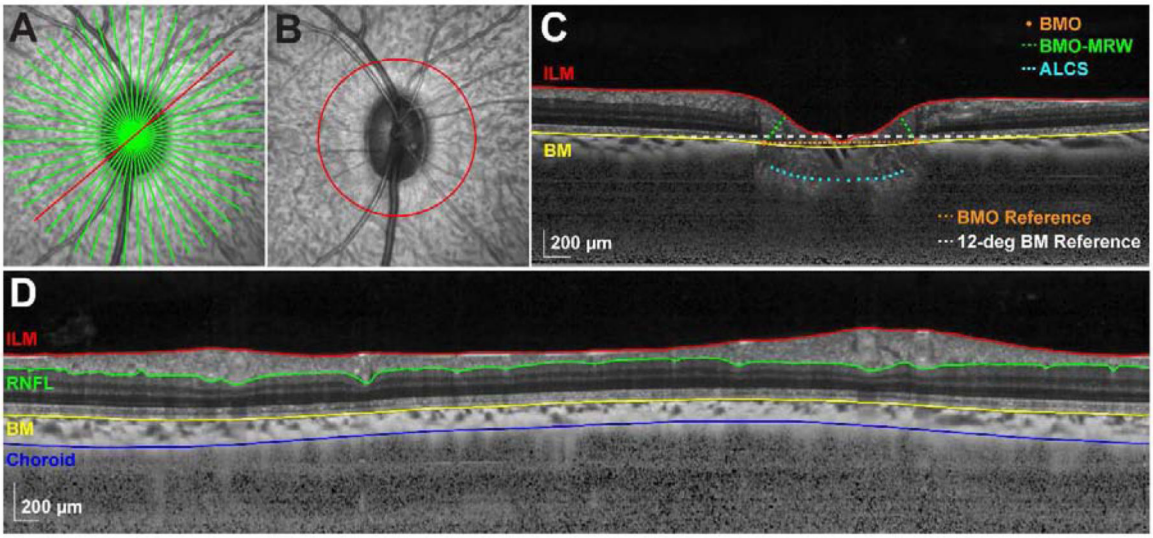

Figure 1. OCT segmentation and anatomical landmarks.

A. 20-degree SLO image depicting a 24-line radial scan through the ONH. B. 20-degree SLO image depicting a 12-degree circular scan. C. Compensated radial B-scan (corresponding with the location of the red line in A and compensated as described by Girard et al., 2011), illustrating ILM and BM segmentations, BMO and ALCS locations, BMO-MRW, and BM and BMO reference planes used for calculating BMO height and BMO-ALCSD, respectively. D. Compensated interpolated B-scan (corresponding with the scan location in B), illustrating ILM, RNFL, BM, and choroid segmentations.

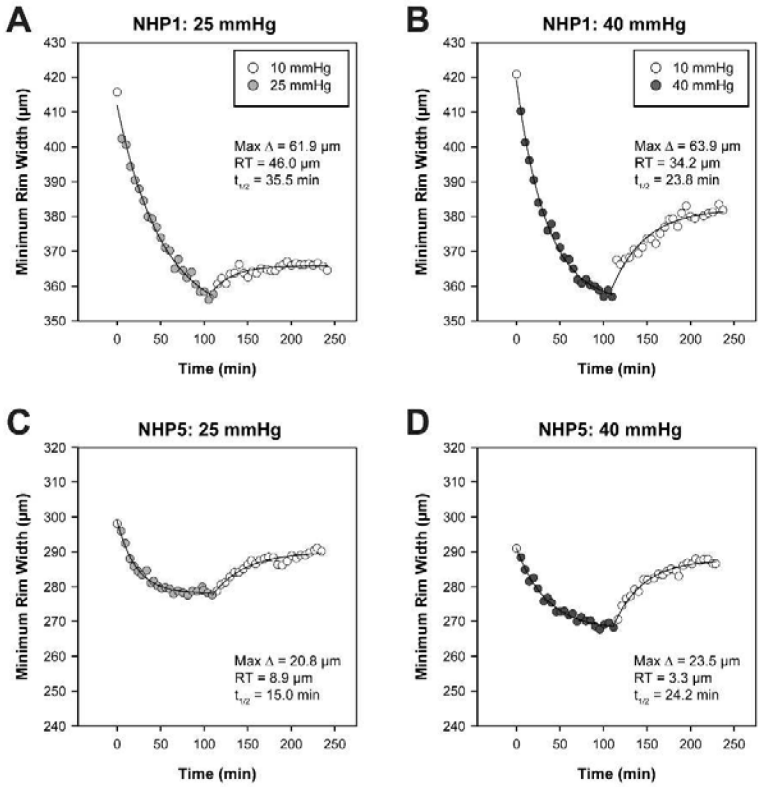

Figure 2. Individual BMO-MRW dynamics with mild and moderate IOP elevation and subsequent reduction.

A. BMO-MRW values quantified every 5 min for the animal with the greatest maximum change in BMO-MRW (NHP1) in response to IOP elevation to 25 mmHg, followed by reduction to 10 mmHg. B. BMO-MRW for NHP1 during the 40 mmHg experiment. For both 25 and 40 mmHg experiments, NHP1 demonstrates substantial residual thinning (RT) of the BMO-MRW. C. BMO-MRW values over time for the animal with the smallest maximum change in BMO-MRW (NHP5) during the 25 mmHg experiment. D. BMO-MRW for NHP5 during the 40 mmHg experiment. NHP5 exhibits a more robust rebound and less RT than NHP1. $t_{1/2}$ = half-life for BMO-MRW thinning.

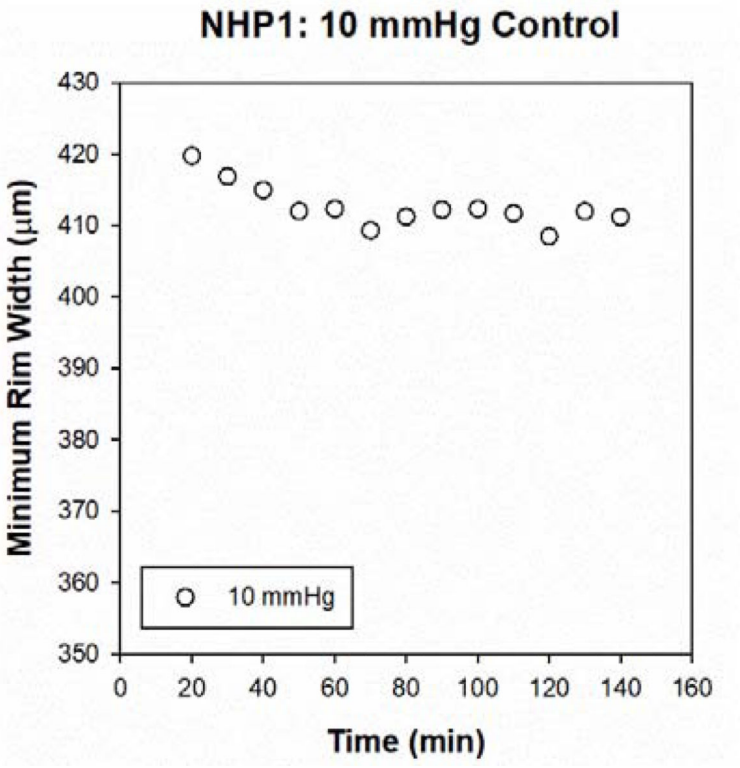

Figure 3. Control cannulation experiment at IOP of 10 mmHg.

BMO-MRW values for NHP1 (animal with the greatest maximum change in BMO-MRW, contralateral eye), starting approximately 20 min after cannulation and quantified every 10 min for 2 hrs. The y-axis scale is the same as Fig 2A&B to facilitate comparison. The decrease in BMO-MRW is approximately 9 μm, compared with decreases of 58 and 64 μm over a similar period of time for the 25 and 40 mmHg experiments, respectively.

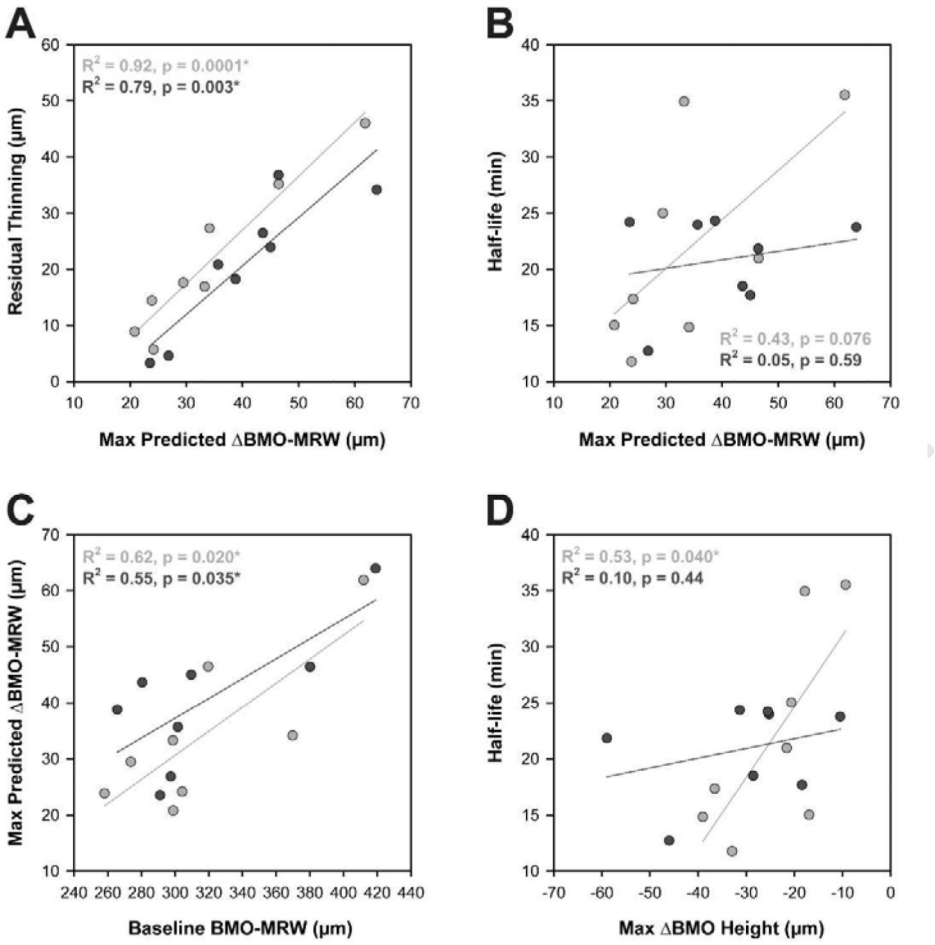

Figure 4. Residual thinning is related to the maximum predicted change in BMO-MRW.

Linear regression relationships between A. residual thinning and maximum predicted change in BMO-MRW, B. half-life and maximum predicted change in BMO-MRW, C. maximum predicted change in BMO-MRW and baseline BMO-MRW, and D. half-life and maximum change in BMO height. Light gray = 25 mmHg experiments, dark gray = 40 mmHg experiments. * denotes statistical significance ($p < 0.05$).

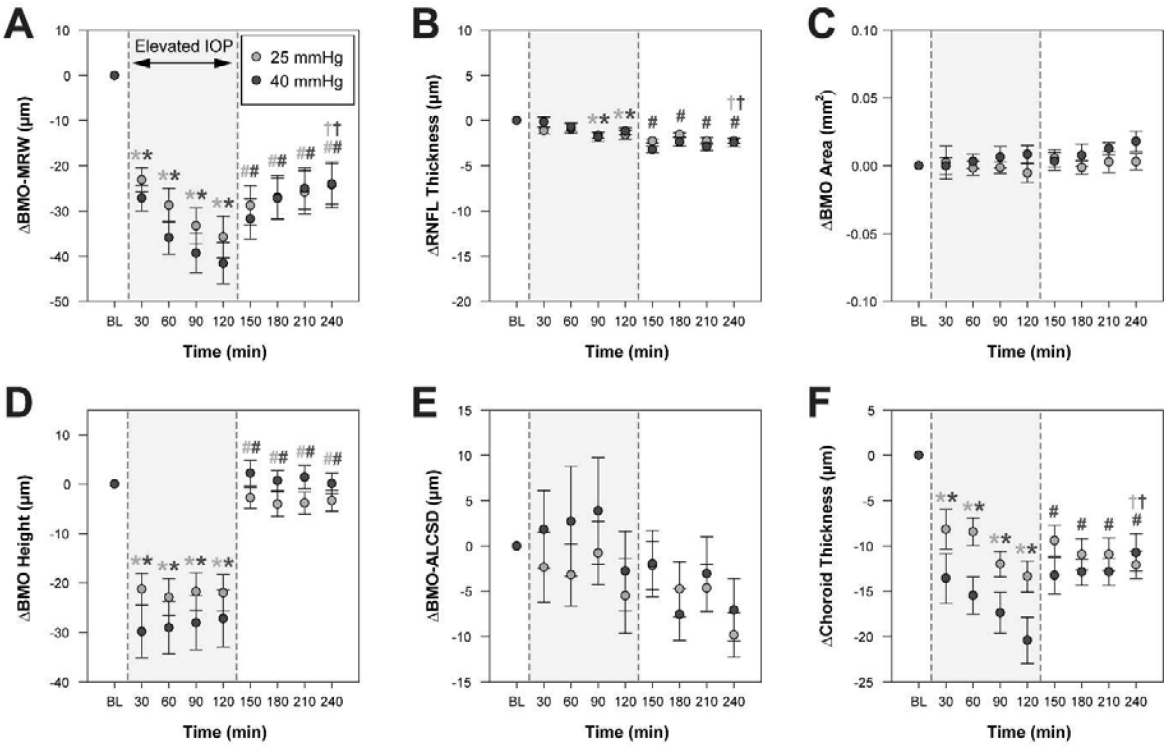

Figure 5. Change in OCT parameters over time during IOP modulation experiments.

Plots illustrate mean difference ± standard error from the final 10 mmHg baseline measure prior to IOP elevation. For comparison with other parameters, BMO-MRW is presented in 30 min intervals. The shaded region shows the period of time over which IOP was elevated to either 25 mmHg or 40 mmHg. Measures during IOP elevation were compared to baseline measures at 10 mmHg, and a statistically significant difference is noted by a light gray and/or dark gray * (light gray * = significant difference for 25 mmHg experiment, dark gray * = significant difference for 40 mmHg experiment). Following IOP reduction to 10 mmHg, measures were compared to the final measure during IOP elevation (i.e., at 120 min), and a statistically significant difference is noted by a light gray and/or dark gray # for the 25 mmHg and 40 mmHg experiments, respectively. A statistically significant difference between endpoint (i.e., 240 min) and baseline is noted by a light gray and/or dark gray † for the 25 mmHg and 40 mmHg experiments, respectively.

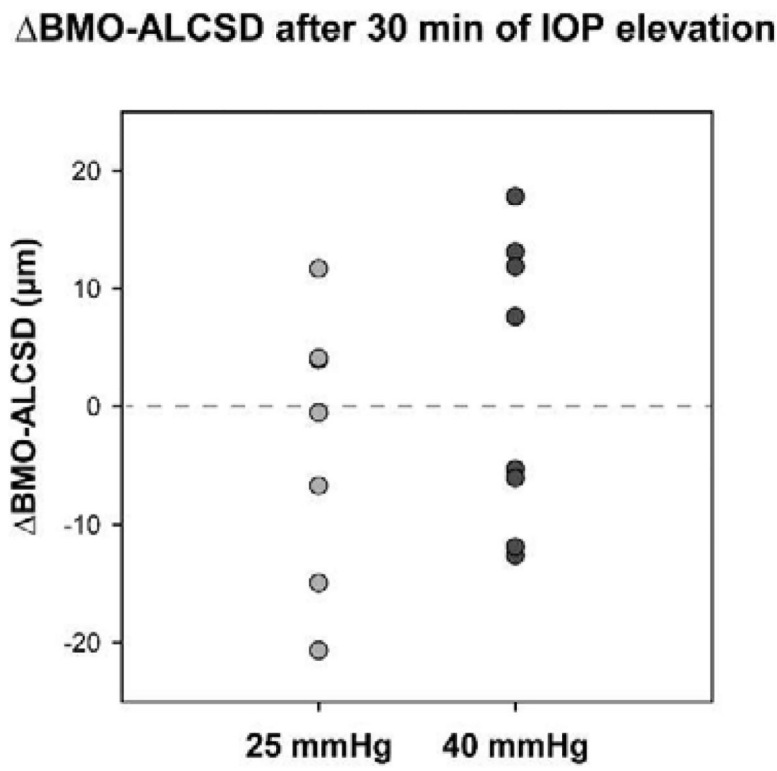

Figure 6. Change in BMO-ALCSD after 30 min of IOP elevation.

The plot shows ΔBMO-ALCSD values for each animal 30 min into IOP elevation to either 25 or 40 mmHg. For both pressure levels, 4 animals exhibited posterior (negative) BMO-ALCSD displacement, whereas the other 4 animals demonstrated anterior (positive) displacement. In animals with posterior movement of the BMO-ALCSD the translaminar pressure difference (IOP – cerebrospinal fluid pressure) was likely the driving force, and anterior movement of the BMO-ALCSD was likely driven by hoop stress and resulting expansion of the scleral canal, pulling the lamina taught and in towards the eye.

Table 1.

Individual BMO-MRW dynamics: Exponential decay and rise to maximum functions

25 mmHg Experiments						
	Exponential Decay (25 mmHg)			Exponential Rise to Maximum (10 mmHg)		
Subject	Baseline BMO-MRW (μm)	Max ΔBMO-MRW (μm)	Half-life (min)	Plateau (μm)	Residual ΔBMO-MRW (μm)	Half-time (min)
NHP1 (M) *	411.9	61.86	35.51	365.9	46	17.09
NHP2 (M) *	273.7	29.45	25.02	256.1	17.6	16.07
NHP3 (M) *	369.8	34.13	14.84	342.5	27.3	26.25
NHP4 (M)	298.7	33.24	34.92	281.8	16.9	115.5
NHP5 (M)	298.9	20.79	15.01	290	8.9	26.29
NHP6 (M) *	319.6	46.47	20.96	284.4	35.2	18.27
NHP7 (F)	304.2	24.14	17.35	298.5	5.7	52.85
NHP8 (F) *	258.1	23.86	11.77	243.7	14.4	52.98
Mean ± SD	316.9 ± 50.7	34.2 ± 13.8	21.9 ± 9.2	295.4 ± 41.0	21.5 ± 13.7	40.7 ± 33.8
40 mmHg Experiments						
	Exponential Decay (40 mmHg)			Exponential Rise to Maximum (10 mmHg)		
Subject	Baseline BMO-MRW (μm)	Max ΔBMO-MRW (μm)	Half-life (min)	Plateau (μm)	Residual ΔBMO-MRW (μm)	Half-time (min)
NHP1 (M)	419	63.9	23.75	384.8	34.2	38.92
NHP2 (M)	280.5	43.64	18.49	254.1	26.4	30.78
NHP3 (M)	380.2	46.42	21.82	343.4	36.8	20.1
NHP4 (M) *	301.6	35.64	23.97	280.8	20.8	35.51
NHP5 (M) *	291.1	23.51	24.21	287.8	3.3	23.34
NHP6 (M)	309.6	45.01	17.68	285.7	23.9	21.87
NHP7 (F) *	297.4	26.84	12.72	292.8	4.6	40.37
NHP8 (F)	265.6	38.77	24.34	247.4	18.2	34.35
Mean ± SD	318.1 ± 53.1	40.5 ± 12.6	20.9 ± 4.2	297.1 ± 45.8	21.0 ± 12.3	30.7 ± 8.0

* Indicates experiment that was performed 1st

Table 2.

Mean ± standard deviation for all parameters, quantified every 30 minutes during IOP modulation

25 mmHg Experiments									
	Baseline	Elevated IOP				Reduced IOP			
		0.5 hr	1 hr	1.5 hrs	2 hrs	2.5 hrs	3 hrs	3.5 hrs	4 hrs
RNFLT (μm)	112.7 ± 5.6	111.5 ± 5.0	111.8 ± 5.0	111.0 ± 5.1	111.1 ± 4.8	110.4 ± 5.2	111.1 ± 5.4	110.4 ± 5.7	110.4 ± 6.0
BMO-MRW(μm)	318.6 ± 51.7	295.5 ± 46.5	289.9 ± 43.7	285.4 ± 43.4	282.9 ± 42.4	289.8 ± 42.5	291.6 ± 41.9	292.8 ± 42.6	294.4 ± 41.7
BMO Area (mm^2)	1.21 ± 0.13	1.21 ± 0.14	1.21 ± 0.13	1.21 ± 0.13	1.20 ± 0.12	1.21 ± 0.12	1.21 ± 0.12	1.21 ± 0.12	1.21 ± 0.13
BMO Height (μm)	−25.8 ± 14.0	−47.1 ± 19.5	−48.8 ± 21.1	−47.6 ± 21.0	−47.8 ± 20.3	−28.6 ± 12.8	−29.9 ± 14.8	−29.7 ± 14.3	−29.2 ± 13.6
BMO-ALCSD (μm)	−202.3 ± 42.4	−204.7 ± 38.4	−205.5 ± 38.0	−203.1 ± 37.7	−207.8 ± 37.8	−204.5 ± 39.2	−207.1 ± 41.7	−207.0 ± 43.2	−212.1 ± 42.4
ChoroidT (μm)	109.4 ± 16.7	101.2 ± 18.2	100.9 ± 16.8	97.3 ± 14.0	96.0 ± 15.4	99.9 ± 16.7	98.4 ± 15.5	98.4 ± 14.7	97.3 ± 14.6
40 mmHg Experiments									
	Baseline	Elevated IOP				Reduced IOP			
		0.5 hr	1 hr	1.5 hrs	2 hrs	2.5 hrs	3 hrs	3.5 hrs	4 hrs
RNFLT (μm)	112.6 ± 5.8	112.4 ± 5.0	111.8 ± 5.5	110.8 ± 5.7	111.4 ± 5.6	109.4 ± 6.3	110.2 ± 5.8	109.7 ± 5.9	110.1 ± 5.7
BMO-MRW (μm)	319.5 ± 53.1	292.3 ± 48.2	283.6 ± 46.3	280.2 ± 45.7	277.9 ± 44.5	287.7 ± 45.0	292.3 ± 45.6	294.4 ± 45.4	295.5 ± 46.2
BMO Area (mm^2)	1.20 ± 0.13	1.20 ± 0.14	1.20 ± 0.13	1.20 ± 0.13	1.21 ± 0.13	1.20 ± 0.13	1.21 ± 0.13	1.21 ± 0.13	1.22 ± 0.13
BMO Height (μm)	−28.9 ± 10.3	−58.8 ± 21.2	−58.0 ± 21.3	−57.0 ± 21.1	−56.2 ± 21.8	−26.7 ± 11.2	−28.2 ± 10.6	−27.6 ± 11.6	−28.8 ± 12.4
BMO-ALCSD (μm)	−203.3 ± 43.7	−201.4 ± 34.3	−200.6 ± 34.0	−199.4 ± 30.4	−206.1 ± 32.4	−205.2 ± 35.4	−210.8 ± 38.4	−206.3 ± 34.7	−210.3 ± 35.9
ChoroidT (μm)	110.1 ± 21.0	96.5 ± 16.0	94.6 ± 17.1	92.7 ± 16.4	89.6 ± 15.4	96.8 ± 16.8	97.2 ± 18.4	97.2 ± 18.5	99.3 ± 19.1

RNFLT = RNFL thickness, ChoroidT = Circumpapillary choroid thickness